Available online at www.sciencedirect.com
ScienceDirect
Polymer 48 (2007) 5259–5267
polymer
www.elsevier.com/locate/polymer

Aligned three-dimensional microstructures of conducting polymer composites

Hua Bai, Chun Li, Feng'en Chen, Gaoquan Shi*

Department of Chemistry and Key Lab of Bio-organic Phosphorous, Tsinghua University, Beijing 100084, People's Republic of China

Received 24 April 2007; received in revised form 21 June 2007; accepted 29 June 2007
Available online 13 July 2007

Abstract

The composites of polypyrrole (PPy) and poly(vinyl alcohol) (PVA) with aligned 3-dimensional (3D) microstructures have been fabricated *via* vapor deposition polymerization (VDP) of pyrrole onto the microstructured composites of PVA and $FeCl_3$ (PVA–$FeCl_3$) formed by directional freezing. In these composites, the microstructures of PVA act as the frameworks and the conducting polymer components provide the materials with conductive function. The composites are foam-like with low weight density. However, they have good mechanical properties, and can be easily mechanically processed into various desired shapes. The apparent conductivity of the composite containing 20 wt% PPy was measured to be approximately 0.1 S cm^{-1}. The ammonia gas sensor based on this 3D composite exhibited high sensitivity. The strategy developed here can be extended to fabricate the 3D microstructured conductive composites by using other conducting polymers or water-soluble polymers.

Keywords: Conducting polymer; Poly(vinyl alcohol); Microstructure

1. Introduction

Micro- and nanostructured conducting polymeric materials have attracted increasing attention, mainly due to their potential applications in catalysis, optics, drug delivery, and microelectronics [1–5]. Various micro- and nanostructured conducting polymers have been successfully synthesized, however, most of them have one or two-dimensional structures [6–18]. Well-defined 3-dimensional (3D) inverse opals of conducting polymers including polypyrrole (PPy), polythiophene, polyaniline and poly(phenylenevinylene) were prepared by polymerizing the corresponding monomers in the colloidal crystal templates [19–21]. However, this sacrificial template method is multiple-stepped and uneconomic because of using and discarding templates. Furthermore, this method is difficult to be applicable to fabricate a microstructured conducting polymeric material with a size of several centimeters.

Recently, Cooper's group successfully prepared 3D microstructures of polymers and polymer/inorganic nanoparticle composites by directional freezing [22]. On the other hand, vapor deposition polymerization (VDP) is a convenient method for fabricating thin conducting polymer films with high electric conductivity on various surfaces [23–26]. Here, we desire to report the fabrication of aligned 3D microstructures of conducting polymer/water-soluble polymer composites by combining these two techniques. In these composites, the microstructures of water-soluble polymers acted as the frameworks of the materials and the conducting polymer components provided the materials with conductive function. These composites showed low apparent weight density, good mechanical property and high electrochemical activity. Furthermore, the ammonia gas sensor based on these 3D composites exhibited high sensitivity.

2. Experimental

2.1. Materials

Poly(vinyl alcohol) with repeat unit number of 2400–2500 (PVA 124, hydrolysis degree 98–99%) and ferric chloride

* Corresponding author. Fax: +86 10 62771149.
E-mail address: gshi@tsinghua.edu.cn (G. Shi).

0032-3861/$ - see front matter © 2007 Elsevier Ltd. All rights reserved.
doi:10.1016/j.polymer.2007.06.071

anhydrous (analytical pure grade) were purchased from Beijing Chem. Reagents Co. (Beijing, China) and used as received. Poly(ethylene glycol) (PEG, chemical pure grade) with molar mass of 20,000 g was purchased from Beijing Yili Fine Chem. Co. Ltd. (Beijing, China), and pyrrole was a product of Sinopharm Chemical Reagents Co. Ltd. (Beijing, China) and was distilled under reduced pressure before use. 3,4-Ethylenedioxythiophene (EDOT, 99.5%) was bought from Aldrich and used without further purification.

2.2. Fabrication of 3D microstructures

The procedure of preparing the 3D microstructures of the conductive composites is described as follows. Firstly, PVA (2.5, 5, 7.5, and 10 wt%) or PEG (5, 10 and 20 wt%) aqueous solution containing 0.1 M $FeCl_3$ was poured into a polypropylene tube, which is 60 mm in length and 10 mm in diameter. The solution was frozen by dipping the tube into liquid nitrogen at a constant rate of 5 mm/min. After freeze-drying the samples, the free-standing composite blocks of the polymer and $FeCl_3$ (PVA–$FeCl_3$ or PEG–$FeCl_3$) with 3D microstructure were obtained. Secondly, the as-prepared PVA–$FeCl_3$ or PEG–$FeCl_3$ composite block was put into a reaction vessel (250 ml) equipped with a sealing apparatus and a monomer loading reservoir. The monomer in the reservoir evaporated gradually and diffused into the polymer–$FeCl_3$ composites where it was polymerized. After VDP of pyrrole for 24 h, the final product was dried under vacuum for 12 h. PVA–PEDOT composite was prepared following the same procedures except that the VDP was carried out at 50 °C to accelerate the reaction.

To partly remove PVA components from the PVA–PPy composites, the composite blocks were soaked in boiling aqueous HCl solution (pH = 1). The maceration was lasted for 4 h, and the water was refreshed every hour. Finally, the composite blocks were taken out and dried slowly in air or freeze-dried.

2.3. Ammonia gas sensing

The sensing behavior of the as-obtained PVA–PPy composite block was characterized by measuring its resistance change upon exposing to NH_3 gas. The composite block was cut into a small piece ($5 \times 3 \times 3$ mm^3) on which two electrodes were attached directly using two metallic clamps. The distance between these two electrodes was 3 mm. This device was fixed into a 500 cm^3 chamber, and two electrodes were connected to a potentiostat model 440A (CHI, USA) under computer control to measure the current changes at a constant applied potential (40 mV) during changing the ammonia concentration in the chamber. Ammonia gas (1000 ppm) and pure nitrogen were delivered to the chamber under the control of two mass flow controllers (MFC) (D07-12/ZM, Beiing Sevenstar Huachuang Electronics Co., Ltd.). The total flux was fixed to be 500 sccm (standard cubic centimeter per minute) while the concentration of ammonia was controlled by changing the flux rate of these two gases.

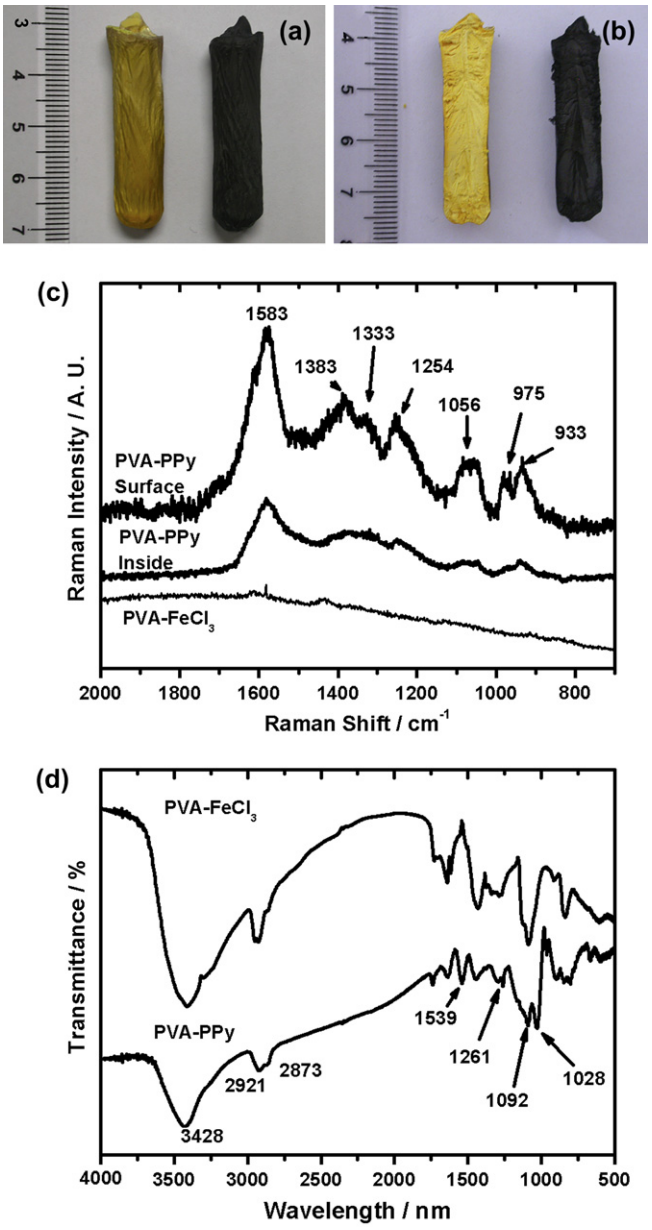

Fig. 1. The optical images and spectra of PVA composite blocks. (a) The overall and (b) the sectional images of PVA–$FeCl_3$ composites before (yellow ones) and after (black ones) VDP of pyrrole for 24 h. (c) Raman and (d) IR spectra of the PVA–$FeCl_3$ and PVA–PPy composites. The PVA–$FeCl_3$ composite block was prepared by directional freezing 5% PVA aqueous solution containing 0.1 M $FeCl_3$. (For interpretation of the references to color in this figure legend, the reader is referred to the web version of this article.)

Before testing, the device had been kept in the chamber under pure nitrogen flow for equilibration until its resistance became stable. For each time, the ammonia flow was supplied for 5 min and then turned off; simultaneously the current change was recorded during this period of ammonia pulse. The temperature of the chamber was kept to be 20 °C and its humidity was measured to be 15%. The sensitivity of the sensor was defined as $(R_g - R_b)/R_0$; where R_0 is the resistance of the device before testing, R_g is the resistance after exposure to the ammonia gas for 300 s and R_b is the instant resistance before

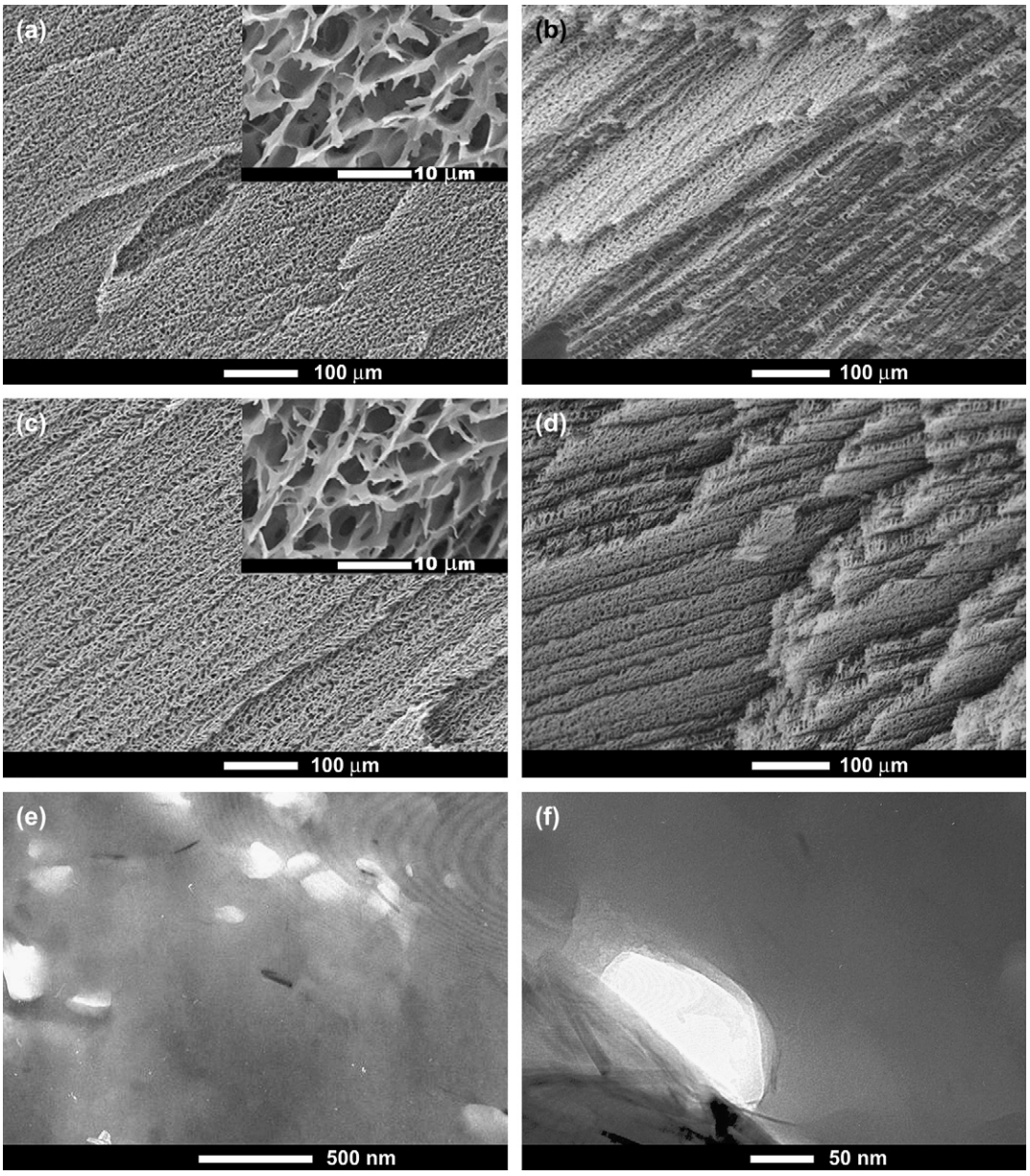

Fig. 2. (a–d) SEM and (e and f) TEM images of PVA composites made from directional freezing. (a and b) PVA–$FeCl_3$ composite prepared by directional freezing 5 wt% PVA solution containing 0.1 M $FeCl_3$. The inset shows magnified view of (a); (c and d) PVA–PPy composite (20 wt% PPy) obtained through VDP of pyrrole onto the PVA–$FeCl_3$ composite matrix shown in panes (a) and (b). The inset shows magnified view of (c); (e and f) TEM images of a slice prepared by microtoming the PVA–PPy composite block shown in pane (c).

injecting ammonia gas. All the resistances were calculated according to the recorded current–time curves.

2.4. Instrumentation

Raman spectra were taken out by the use of an RM 2000 microscopic confocal Raman spectrometer (Renishaw PLC, England) employing a 633-nm laser beam, and a charge coupled device detector with 4 cm^{-1} resolution. The spectra were recorded by focusing a 1–2 μm laser spot on the sample with a 20× objective and accumulated 3 times for 30 s each. IR spectra were taken out on a GX Fourier transform infrared (FTIR) spectrometer (Perkin–Elmer) with KBr pellets of the composites. Since the composites were difficult to be ground into fine powders due to their tenacity, they were dipped into water for several minutes to soften it and then ground with KBr, finally they were well dried and pressed into pellets. The morphologies of the composites were imaged with a scanning electron microscope (SEM, KYKY 2800, China), operated at 25 kV. For SEM examinations, the composite blocks were cut into pieces with a knife. The newly formed cross-sections of the composites without PPy were sputtered with a thin layer of gold, while those of the composites containing PPy were used directly because of their high conductivity. The transmission electron microscopic (TEM) images were taken out using a HITACHI H-800 electron microscope and the

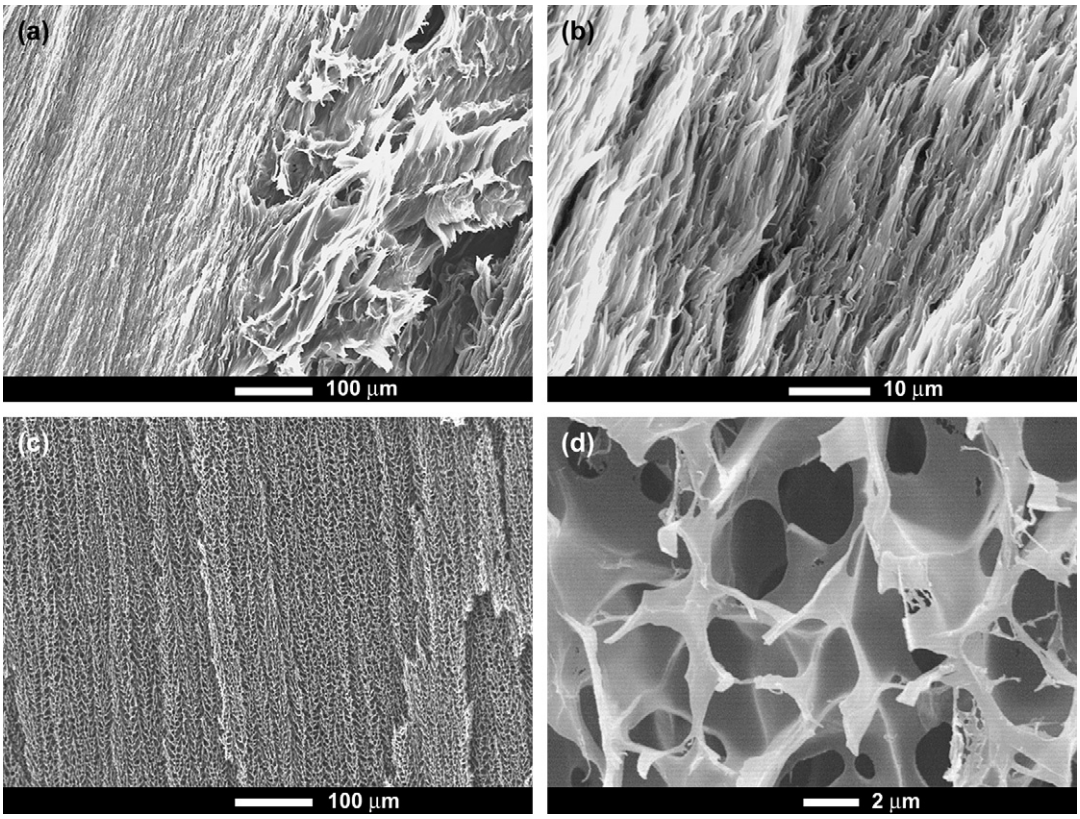

Fig. 3. SEM images of the PVA–PPy composites (28 wt% PPy) after macerated in boiling aqueous HCl solution (pH = 1). (a and b) Dried in air; (c and d) freeze-dried. Panes (b) and (d) are the magnified views of panes (a) and (c), respectively.

samples' slices were prepared by microtoming PVA–PPy composite. Electrochemical measurements were performed with a 273A potentiostat (EG&G), and the reference electrode was an Ag/AgCl wire. Elemental analysis was carried out by using a CE-400 elemental analyzer (EAI, USA). Tensile strength was measured by using a uniaxial tension tester model AGS-10KNG (SHIMADZU).

3. Results and discussion

The 3D microstructured PVA–$FeCl_3$ composite formed by directional freezing the aqueous solution of 5% (by weight) PVA and 0.1 M $FeCl_3$ is yellow in color because of the presence of $FeCl_3$. However, its color was changed to black after VDP of pyrrole onto this matrix (Fig. 1a and b), indicating the formation of PVA–PPy composites. The content of PPy in the composite formed by VDP of pyrrole onto the PVA–$FeCl_3$ composite matrix described above for 24 h was calculated to be about 20 wt% according to the results of elemental analysis (C: 45.15%, H: 6.96%, N: 4.93%) and mass increase of the composite block caused by polymerization. This value was higher than that of quantitative calculation result based on the feeding $FeCl_3$ amount. This is possibly due to that the oxygen in air took part in the reaction, either directly oxidized pyrrole to PPy or transforming Fe^{2+} to Fe^{3+}. PPy content in the composite can be modulated by the VDP time and the concentration of $FeCl_3$ in PVA solution. The apparent weight density of PVA–PPy composite was measured to be 0.07 g cm^{-3}, indicating that the composite is a foam-like material. However, this composite has good mechanical properties, and can be easily mechanically processed into various desired shapes. The tensile strength and elongation at break of the composite were measured to be 2.0 ± 0.2 MPa and $4 \pm 0.5\%$, respectively. The apparent *d.c.* conductivity of the composite was measured by conventional four-electrode technique to be approximately 0.1 S cm^{-1}. Considering the porous structure of the material with low weight density, the conductivity of the walls of the network was evaluated to be about 1.4 S cm^{-1}. This value is comparable to that of the interpenetrating polymer network composites of PPy and poly(methyl acrylate) or poly(styrene-*co*-butyl acrylate) [27].

The formation of PPy has been confirmed by Raman and IR spectra. Fig. 1c shows the Raman spectra recorded on the surface and the cross-section of the PVA–PPy composite. It can be seen that both spectra exhibit the typical characteristic bands of PPy [28,29], and the relative intensity differences are mainly due to the roughness and material amount differences of these two surfaces. The 1583 cm^{-1} band can be assigned to the C=C stretching mode of PPy backbones [28,29]. The bands at around 1383 and 1333 cm^{-1} are associated with the ring stretching of PPy, and the double peaks centered at 1056 cm^{-1} are attributed to C–H in-plane deformation. Bands at 975 and 933 cm^{-1} are assigned to the ring deformation related to bipolarons and polarons,

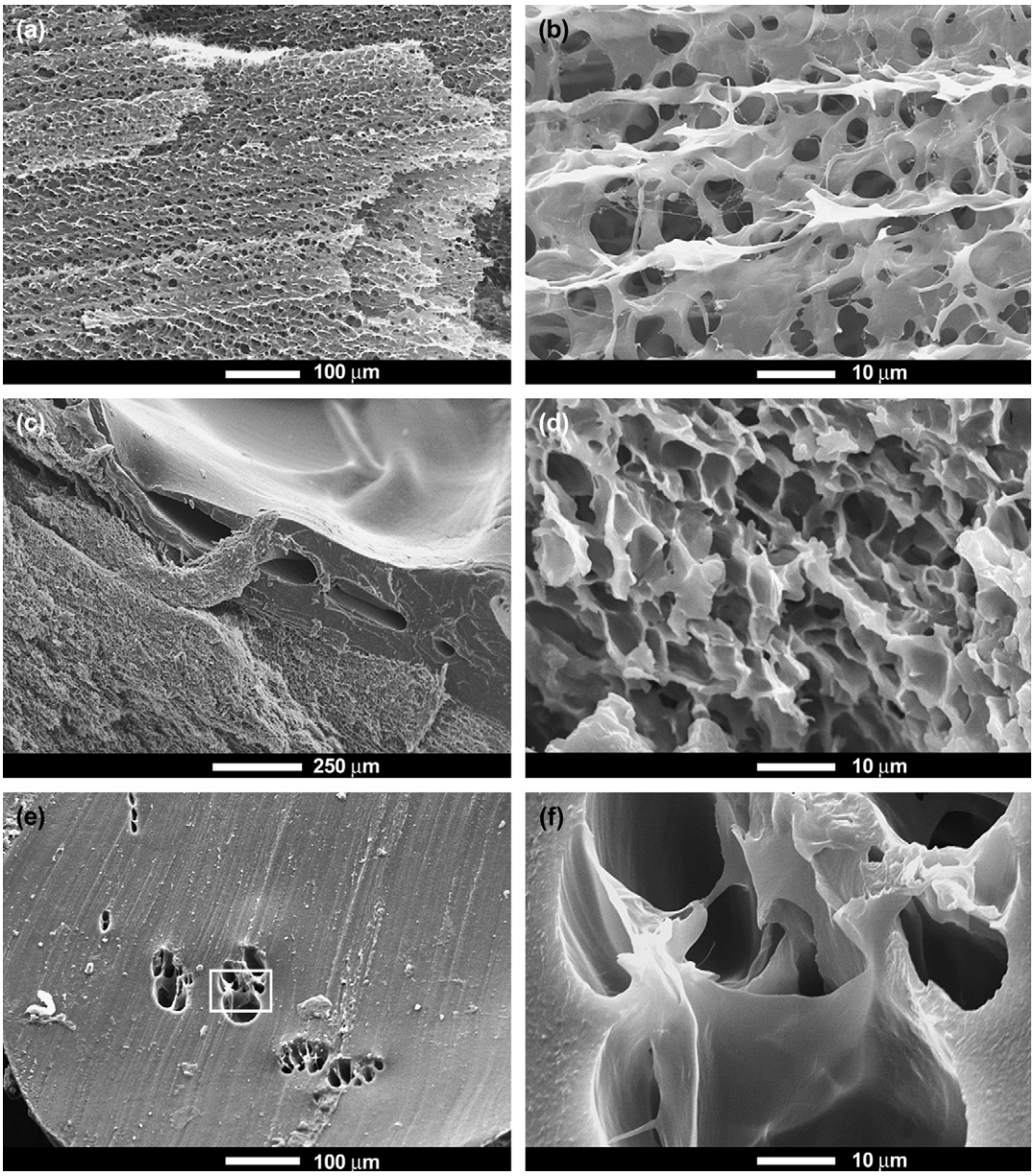

Fig. 4. SEM images of the PVA–PPy composites templated by PVA–$FeCl_3$ 3D microstructure matrix fabricated from the PVA solutions with different concentrations. (a and b) From 2.5 wt% PVA solution (30% wt PPy); (c and d) from 7.5 wt% PVA solution (7 wt% PPy); (e and f) from 10 wt% PVA solution (7 wt% PPy), (f) a magnified image of rectangle area in (e).

respectively [29]. It should be noted here that the Raman spectrum of PVA–$FeCl_3$ composite showed only two weak bands related to –OH and $-CH_2$ groups in the same spectral range (Fig. 1c). In the IR spectrum (Fig. 1d), some bands of PPy are overlapped with those of PVA, and only a few peaks can be distinctly assigned to PPy. The strong and broad peak at 3428 cm^{-1} belongs to –OH groups of PVA or trace amount of water. The peaks at 2921 and 2873 cm^{-1} are ascribed to the $-CH_2$ groups of PVA, while the peak at 1092 cm^{-1} is assigned to C–O stretching of PVA, which can also be found in the spectrum of PVA–$FeCl_3$. The 1539, 1261 and 1028 cm^{-1} peaks are related to PPy, and can be attributed to the C=C stretching, ring deformation of pyrrole and in-plane bending of C–H bonds, respectively [30].

Fig. 2a and b is the typical SEM images of PVA–$FeCl_3$ 3D microstructures formed by freeze-drying the aqueous solution of 5% PVA and 0.1 M $FeCl_3$. The periodic structure can be interpreted as the result of phase separation during the directional freezing process. Freezing the aqueous solution of PVA caused constitutional supercooling at the water/ice interface, leading to Mullins–Sekerka instability and ice cell growth with a well-defined wavelength [31–33]. Therefore, the polymer component was concentrated in the template of ice cells and finally forms microstructure after removing water by freeze-drying [22]. In this study, $FeCl_3$ is mixed with the polymer to construct a homogeneous PVA–$FeCl_3$ composite. There is an aligned accumulation of spongy panels in the material, and the panels are parallel to the axis of the cylindrical

block. The panels are connected with each other by smaller sub-structures, so the frameworks of the composites are 3D networks. Fig. 2c and d illustrates the SEM images of the aligned 3D microstructures of PVA–PPy composites formed by VDP of pyrrole onto the PVA–$FeCl_3$ 3D microstructured matrix as shown in Fig. 2a and b. It is clear from these figures that the PVA–PPy composite kept the microstructures of PVA–$FeCl_3$ matrix after VDP. Usually, VDP will lead to the formation of a core-shell composite structure. However, the TEM images (Fig. 2e and f) of a freeze slice of PVA–PPy composite showed a uniform morphology without phase separation. Thus, it is reasonable to conclude that the walls of the networks are made of a homogeneous blend of PPy and PVA. This is possibly due to that the pyrrole vapor was diffused into the 3D microstructures and polymerized by oxidation with $FeCl_3$.

The PVA component in the composites can be partly removed by soaking the samples in aqueous HCl solution. The lixivium is yellow in color, characteristic of aqueous Fe^{3+}. The shape of the composite block shown in Fig. 1 was maintained during maceration, but shrank to about 30% of its original size after drying in air. SEM images (Fig. 3a and b) exhibit that the microstructure collapsed and the spongy panels huddled together. However, if the macerated block was frozen and then freeze-dried, the microstructures of the composites could be maintained as shown in Fig. 3c and d. The deformities in the microstructures shown in Fig. 3d were caused by the removal of 30% PVA. The conductivity of soaking treated block was decreased to 0.01 S cm^{-1}, and Raman spectral results showed that the PPy component in the composite was in de-doped state. However, its conductivity can be resumed through iodine vapor doping.

Fig. 4 illustrates the SEM images of the PVA–PPy composites prepared by using the PVA–$FeCl_3$ 3D microstructured matrixes made from the aqueous solutions with different concentrations of PVA. As 2.5 wt% PVA solution was used, the microstructure of the resulting PVA–PPy composite (Fig. 4a and b) was similar to that of the composite prepared from the 5 wt% PVA solution shown in Fig. 2. However, the apparent density of the composite was decreased to be only 0.03 g/cm^3. This is mainly due to that the total amount of PVA put in the container for directional freezing was decreased with decreasing PVA concentration, while the apparent volume of the resulting block was almost not changed (decided by the shape of the container). The PPy content in this composite was measured to be about 30%. In contrast, it was found that an inerratic structure could not be prepared from a 7.5 wt% PVA solution. The PVA–$FeCl_3$ composite made from this solution shrank obviously after freeze-drying and their toughness and mechanical strength were much higher than those made from the solutions with lower PVA concentrations. In this case, part of the PVA–$FeCl_3$ block was a highly viscous gel. This gel reacted with pyrrole to form a compact composite as shown in Fig. 4c and d. The PPy content in the composite was measured to be only 7%. This is mainly due to that the compact matrix of PVA–$FeCl_3$ composite restricted the diffusion of the monomer. The composites fabricated from 10 wt% PVA solution did not show any ordered porous structures in micrometer scale. As shown in Fig. 4e and f, the cross-section of the material is compact with only a few holes, and the inner surfaces of the holes are smooth. This is mainly due to the fact that a concentrated PVA solution resulted in inefficient phase separation during directional freezing. The block has a high tensile strength (>5.4 MPa) and large elongation at break (>50%) while a fairly low conductivity (10^{-5} S cm^{-1}). The content of PPy in the resulting composite was also measured to be about 7%.

Fig. 5 shows the cyclic votammograms of a piece of free-standing PVA–PPy composite block (2.3 mg) and a PPy film (1 mg, 1.8 cm^2, deposited on a platinum electrode from an aqueous solution of 0.1 M pyrrole and 0.1 M $LiClO_4$) in 0.1 M acetonitrile solution of tetrabutylammonium tetrafluoroborate (TBATFB). As can be seen from Fig. 5a, the CV of the composite block showed broad and strong capacitive redox waves. Their wave currents were much stronger than those of the flat film deposited on platinum electrode (Fig. 5b). These stronger redox waves are consistent with those of other PPy microstructure and mainly due to the fact that the specific surface area of the composite block is much larger than that of a normal film, which resulted in much higher PPy/electrolyte double-layer capacitive charges [7]. The discharge capacity of the composite film was measured to be about quadruple that of a normal PPy film.

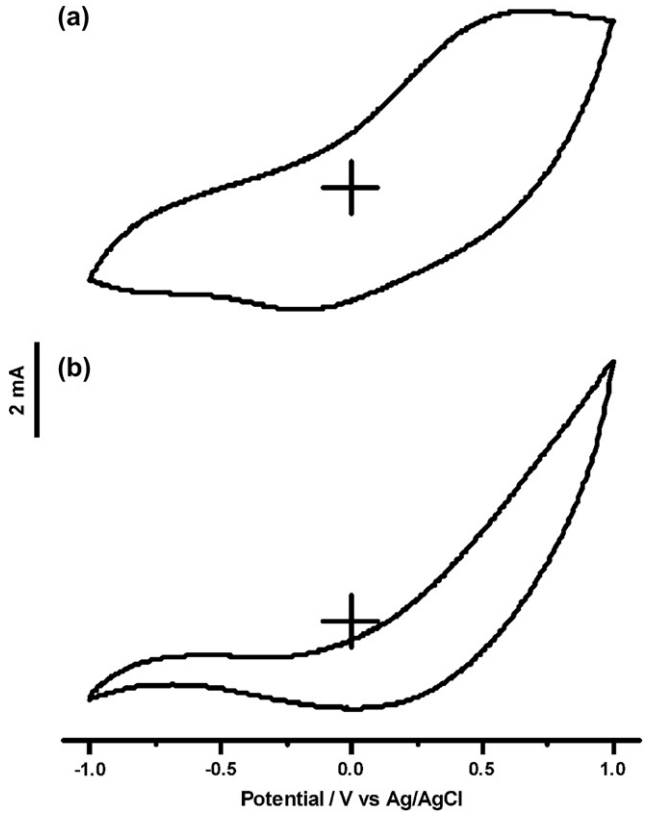

Fig. 5. Cyclic votammograms of (a) the PVA–PPy composite and (b) a flat PPy film in 0.1 M acetonitrile solution of TBATFB at a potential scan rate of 30 mV/s.

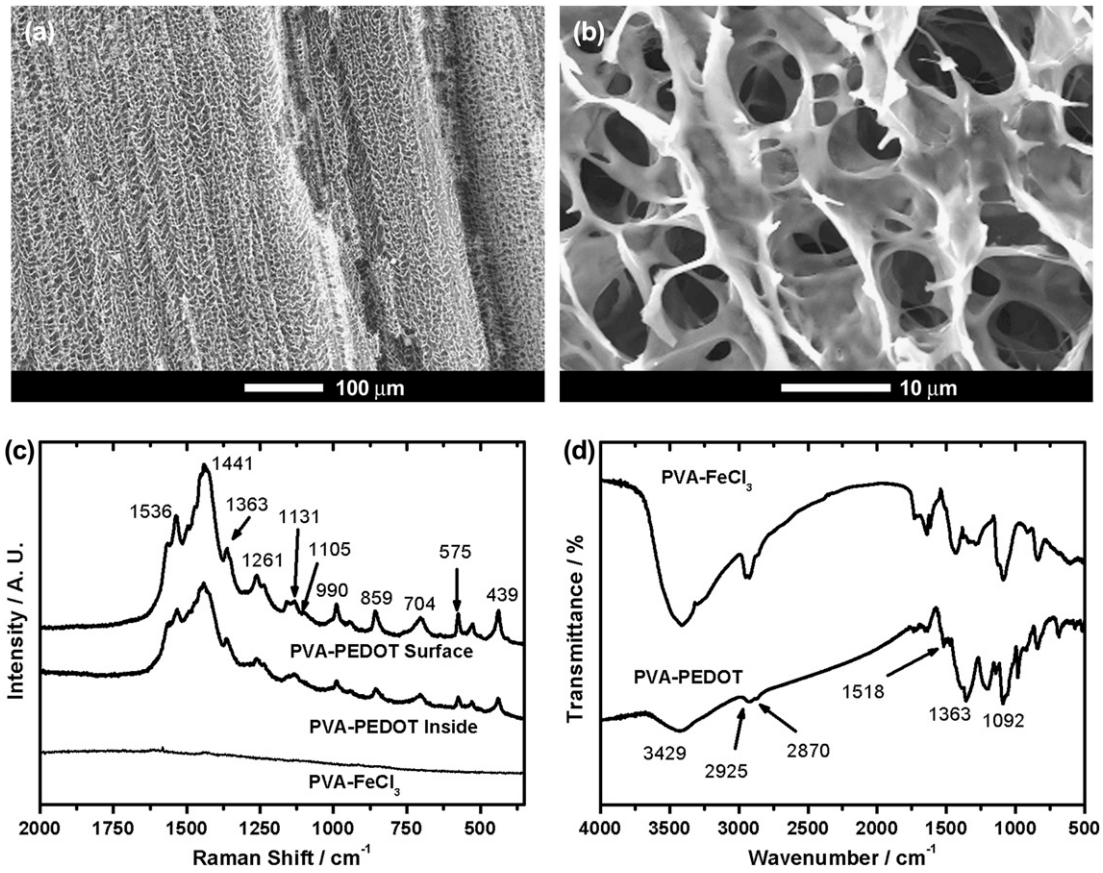

Fig. 6. (a and b) SEM images of the PVA−PEDOT composite (16 wt% PEDOT) fabricated by VDP of EDOT on the microstructured PVA−$FeCl_3$ composite made from 5 wt% PVA solution containing 0.1 M $FeCl_3$; (c) Raman and (d) IR spectra of the PVA−PEDOT composite.

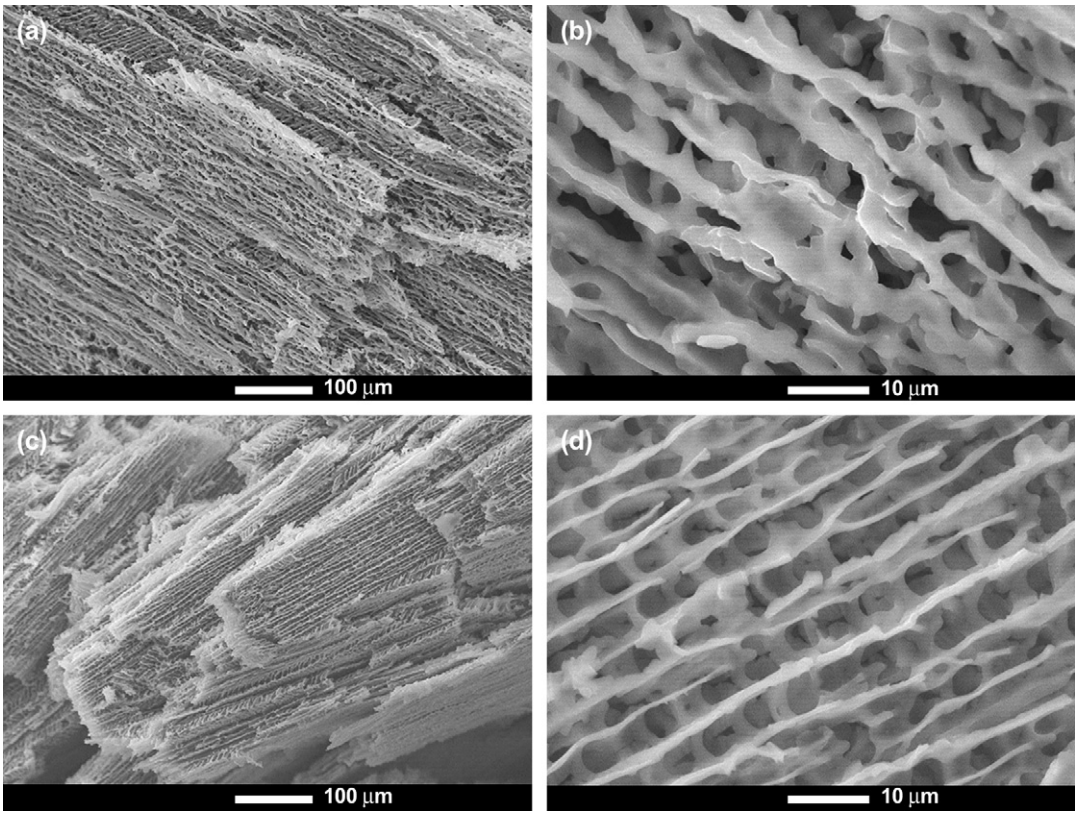

Fig. 7. SEM images of the PEG−PPy composites prepared by VDP of pyrrole at the PEG−$FeCl_3$ composites prepared from the aqueous solution of (a and b) 10 wt% or (c and d) 20 wt% PEG containing 0.1 M $FeCl_3$.

To check whether the strategy developed here is applicable to fabricating composites with other components, we used different monomers and water-soluble polymers to produce the composites. It was found that other aromatic monomers which can be directly oxidative polymerized by $FeCl_3$ are also can be used for producing corresponding conjugated polymer composites with similar 3D microstructures. Fig. 6 shows the SEM images of the composites of poly(3,4-ethylenedioxythiophene) and PVA (PVA–PEDOT) prepared by the same procedure. The vapor pressure of 3,4-ethylenedioxythiophene (EDOT) is lower than that of pyrrole but the oxidation potential is higher [34]. Therefore the polymerization reaction was carried out at 50 °C to accelerate the reaction. As shown in Fig. 6a and b, the microstructure of PVA–PEDOT is almost the same as that of PVA–PPy composite. The Raman and IR spectra (Fig. 6c and d) of PVA–PEDOT indicated that PEDOT was formed inside the block [35,36]. In the Raman spectra, the 1441 cm^{-1} and 1533 cm^{-1} bands are assigned to C=C stretching of thiophene rings, while the bands at 1363, 1131 and 1105 cm^{-1} are attributed to stretching of C–C single bonds. The bands at 1261 and 990 cm^{-1} are associated with C–S stretching and the 704 cm^{-1} band is related to C–S–C deformation. The three bands at 859, 575 and 439 cm^{-1} are assigned to C–O–C vibration of oxyethylene rings. In the IR spectrum, the strong and broad peak at 3429 cm^{-1} belongs to –OH groups of PVA or trace amount of water. The peaks at 2925 and 2870 cm^{-1} are assigned to the $-CH_2$ groups of PVA and oxyethylene ring. The weak peak at 1518 cm^{-1} is ascribed to C=C stretching in thiophene rings, while the wide bands at 1363 and 1092 cm^{-1} belong to CH bending and C–O stretching of both PVA and PEDOT, respectively. The PEDOT content of the composite was calculated to be 16%, which was lower than that of the corresponding PVA–PPy composite. The apparent conductivity of this material was measured to be 0.1 S cm^{-1}.

The framework of the conductive microstructured composites also can be replaced by other water-soluble polymers. Here, poly(ethylene glycol) (PEG) with molar mass of 20,000 g was used. As shown in Fig. 7, the PEG–PPy composites prepared from the solutions of 10 wt% (or 20%) PEG and 0.1 M $FeCl_3$ have microstructures similar to those of the PVA–PPy composites shown in Fig. 2.

PPy has been used to fabricate ammonia gas sensor for several years [37–40]. The 3D network material is expected to have a better performance because of its relative high surface area than normal film. Fig. 8 illustrates the response curves of an ammonia sensor based on the 3D microstructured composite film. After exposed to ammonia gas, the electrical conductivity of the sample decreased dramatically (Fig. 8a). This is mainly due to that the electron donating ammonia reduced the charge carrier density of PPy. The fitting of sensitivity to ammonia concentration gave a line with slope as high as 2.29×10^{-4}/ppm (relative coefficient = 0.99, Fig. 8b). In general, the slope of the line can be used to evaluate the sensitivity of a gas sensor; the value obtained above was much higher than that of a thin PPy film by electrochemical deposition [38], and almost twice that of the device based on a Langmuir–Blodgett PPy film (1.28×10^{-4}) [37].

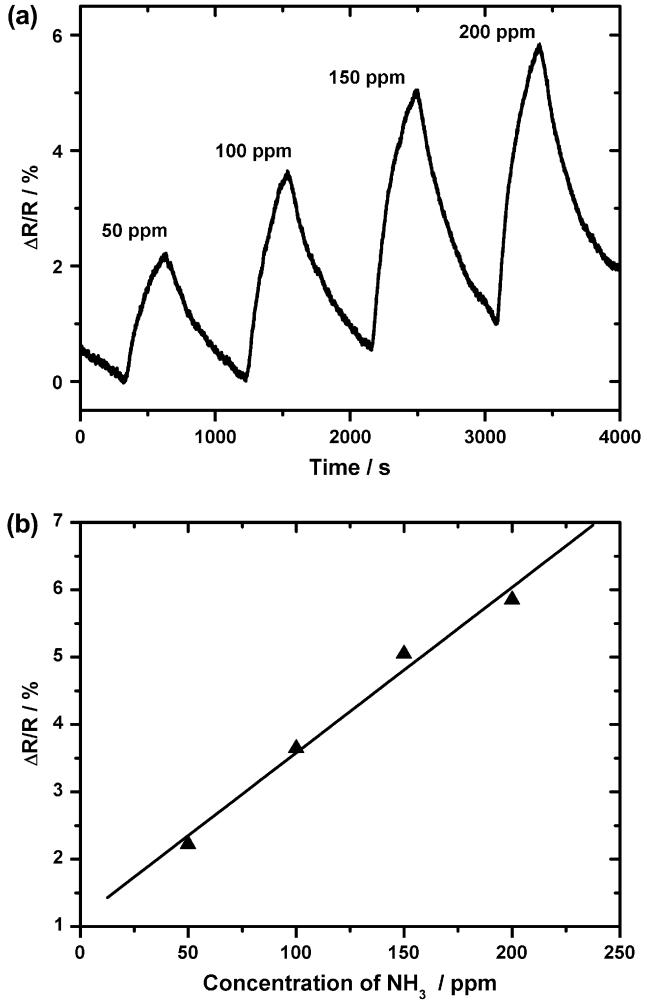

Fig. 8. (a) Ammonia-concentration-dependent resistance response of a sensor based on the PVA–PPy 3D microstructured composite shown in Fig. 2; (b) plot of peak value *vs.* ammonia concentration in (a).

4. Conclusions

In conclusion, PVA–PPy composites with aligned 3D microstructures can be easily fabricated by vapor polymerization of pyrrole onto the PVA–$FeCl_3$ composite formed by directional freezing. The composite shows broad and strong redox responses and can be applied to fabrication of capacitors with high energy density. The ammonia gas sensor based on this material also has high sensitivity. The technique developed here can be extended to fabricate other conducting polymer composites with similar microstructures by using different water-soluble polymers (e.g. polyethylene glycol) or aromatic monomers (e.g. 3,4-ethylenedioxythiophene). This is the first example of fabricating 3D microstructured conducting polymer composites through a template-less approach.

Acknowledgements

This work was supported by National Natural Science Foundation of China (50533030), 973 project (2003CB615700) and 863 project (2006AA03Z105).

References

[1] Ozaki M, Shimoda Y, Kasano M, Yoshino K. Adv Mater 2002;14:514.
[2] Martin CR, Kohli P. Nat Rev Drug Discov 2003;2:29.
[3] Virji S, Fowler JD, Baker CO, Huang JX, Kaner RB, Weiller BH. Small 2005;1:624.
[4] Donley CL, Zaumseil J, Andreasen JW, Nielsen MM, Sirringhaus H, Friend RH, et al. J Am Chem Soc 2005;127:12890.
[5] Abidian MR, Kim DH, Martin DC. Adv Mater 2006;18:405.
[6] Fu MX, Zhu YF, Tan RQ, Shi GQ. Adv Mater 2001;13:1874.
[7] Qu LT, Shi GQ, Chen F, Zhang JX. Macromolecules 2003;36:1063.
[8] Wu XF, Shi GQ. J Mater Chem 2005;15:1833.
[9] Lu GW, Li C, Shi GQ. Polymer 2006;47:1778.
[10] Gao YY, Zhao L, Li C, Shi GQ. Polymer 2006;47:4953.
[11] Yang YS, Wan MX. J Mater Chem 2001;11:2022.
[12] Yang YS, Wan MX. J Mater Chem 2002;12:897.
[13] Zhang ZM, Sui J, Zhang LJ, Wan MX, Wei Y, Yu LM. Adv Mater 2005;17:2854.
[14] Li C, Hatano T, Takeuchi M, Shinkai S. Chem Commun 2004;2350.
[15] Bajpai V, He PG, Dai LM. Adv Funct Mater 2004;14:145.
[16] Zhang XY, Goux WJ, Manohar SK. J Am Chem Soc 2004;126:4502.
[17] Zhong WB, Liu SM, Chen XH, Wang YX, Yang WT. Macromolecules 2006;39:3224.
[18] Konyushenko EN, Stejskal J, Trchova M, Hradil J, Kovarova J, Prokes J, et al. Polymer 2006;47:5715.
[19] Deutsch M, Vlasov YA, Norris DJ. Adv Mater 2000;12:1176.
[20] Cassagneau T, Caruso F. Adv Mater 2002;14:34.
[21] Tian SJ, Wang JJ, Jonas U, Knoll W. Chem Mater 2005;17:5726.
[22] Zhang HF, Hussain I, Brust M, Butler MF, Rannard SP, Cooper AI. Nat Mater 2005;4:787.
[23] Mohammadi A, Lundström I, Salaneck WR, Inganäs O. Chemtronics 1986;1:171.
[24] Kim J, Sohn D, Sung Y, Kim ER. Synth Met 2003;132:309.
[25] Kim J, Kim E, Won Y, Lee H, Suh K. Synth Met 2003;139:485.
[26] Nair S, Natarajan S, Kim SH. Macromol Rapid Commun 2005;26:1599.
[27] Mandal TK, Mandal BM. Synth Met 1996;80:83.
[28] Furukawa Y, Tazawa S, Fujii Y, Harada I. Synth Met 1988;24:329.
[29] Chen F, Shi GQ, Fu MX, Qu LT, Hong XY. Synth Met 2003;132:125.
[30] Costantini N, Lupton JM. Phys Chem Chem Phys 2003;5:749.
[31] Butler MF. Cryst Growth Des 2001;1:213.
[32] Butler MF. Cryst Growth Des 2002;2:541.
[33] Mukai SR, Nishihara H, Tamon H. Chem Commun 2004;874.
[34] Groenendaal BL, Jonas F, Freitag D, Pielartzik H, Reynolds JR. Adv Mater 2000;12:481.
[35] Łapkowski M, Proń A. Synth Met 2000;110:79.
[36] Neugebauer H. J Electroanal Chem 2004;563:153.
[37] Penza M, Milella E, Alba MB, Quirini A, Vasanelli L. Sen Actuators B 1997;40:205.
[38] Bidan G. Sen Actuators B 1992;6:45.
[39] Maksymiuk K. Electroanalysis 2006;18:1537.
[40] Bai H, Shi GQ. Sensors 2007;7:267.